Published in final edited form as:
Biosens Bioelectron. 2011 May 15; 26(9): 3755–3760. doi:10.1016/j.bios.2011.02.021.

Edge-Plane Microwire Electrodes for Highly Sensitive H_2O_2 and Glucose Detection

Liangliang Qiang[1], **Santhisagar Vaddiraju**[1,2], **Dipesh Patel**[1], and **Fotios Papadimitrakopoulos**[1,3]

[1]Nanomaterials Optoelectronics Laboratory, Polymer Program, Institute of Materials Science, University of Connecticut, Storrs, CT 06269

[2]Biorasis Inc., 23 Fellen Road, Storrs, CT 06268

[3]Department of Chemistry, University of Connecticut, Storrs, CT 06269

Abstract

The promise of implantable electrochemical sensors is often undermined by the critical requirement of device miniaturization that inadvertently degrades sensor performance in terms of sensitivity and selectivity. Herein, we report a novel miniaturized and flexible amperometric sensor grown at the 'edge plane' of a 25-μm gold wire. Such geometry affords extreme miniaturization along with ease of fabrication, minimal iR drop and 3-D diffusion for effective mass transfer. This together with electrochemical rebuilding of the Au working electrode and subsequent Pt nanoparticles deposition resulted in the highest H_2O_2 sensitivity (33 $mA \cdot mM^{-1} \cdot cm^{-2}$), reported thus far. Concurrent electrodeposition of *o*-phenylenediamine with glucose oxidase afforded glucose detection at these edge-plane microsensors with a six fold improvement in sensitivity (1.2 $mA \cdot mM^{-1} \cdot cm^{-2}$) over previous reports. In addition, these sensors exhibit low operation potential (0.3 V), high selectivity (more than 95%) against *in vivo* interferences, and an apparent Michealis-Menten constant (K_m^{app}) of 17 and 75 mM of glucose in the absence and presence of an outer polyurethane coating, respectively. These features render the edge-plane sensor architecture as a powerful platform for next-generation implantable biosensors.

Keywords

Glucose; Hydrogen peroxide (H_2O_2) Biosensor; Miniaturization; Electrochemical

1. Introduction

A growing amount of research and clinical work indicates that continuous metabolic monitoring holds great promise for early detection and care of various body disorders and

Correspondence to: Fotios Papadimitrakopoulos.

chronic diseases. (Wilson and Gifford 2005) For instance, continuous glucose monitoring is crucial for diabetes management, (Klonoff 2005) while continuous assessment of lactate and other metabolites in brain has important implications in the study of obesity, shock, sepsis and congested heart failure. (Allen 2000; Wilson and Gifford 2005) While a number of biosensing technologies are currently evaluated, (Vaddiraju et al. 2010; Wang 2007; Wilson and Gifford 2005) enzymatic-based electrochemical methods present a promising venue for transposing the concentration of a given metabolite to an electroactive species (*i.e.* H_2O_2, O_2, etc.) and subsequently sensing it amperometrically. (Vaddiraju et al. 2010; Wilson and Gifford 2005)

On the other hand, in order to minimize the trauma inflicted during sensor implantation, device miniaturization has become particularly important. (Li et al. 2007; Vaddiraju et al. 2010) Miniaturization, however, stands as a major impediment for amperometric techniques, since reduction in the area of the working electrode generally leads to weaker signal intensity that rapidly approaches noise level. To mitigate this challenge, miniaturized amperometric biosensors are constantly advancing the following four research frontiers:

- **i.** Enhancement of surface area of the working electrodes by increasing nanoporosity using metal etching and decorating techniques,(Erlebacher et al. 2001),(You et al. 2003) conducting polymers (Singh et al. 2009), carbon nanotubes,(Yu et al. 2006) and various nanostructured semiconductors. (Singh et al. 2009)
- **ii.** Enhancement of electrocatalytic activity of the working electrode, using a diversity of catalytic schemes that together with appropriate surface reconstruction, impart improved selectivity towards a particular analyte. (Vaddiraju et al. 2010)
- **iii.** Methodologies to increase enzyme loading (*i.e.* layer-by-layer assembly (Wu et al. 2007), hydrogels,(Ahmad et al.) sol-gel (Chen et al. 2002a), nanotubes (Yu et al. 2006), nanoplatelets (Lu et al. 2008), *etc.*) that together with enhanced enzyme stability (Kumar and Chaudhari 2003) and increased turnover rate (Patolsky et al. 2004), provide a significant improvement in sensor performance.
- **iv.** Facilitate better mass transfer and 3-D diffusion of analytes and redox reactants to the working electrodes via the use of ultramicroelectrodes (McMahon et al. 2005) and their arrays. (Hye Jin et al. 2001)

While each of the aforementioned strategies is focused on specific aspects of device performance, the challenge to sensor miniaturization is rarely addressed holistically. In addition, device miniaturization often requires considerable processing sophistication and advanced manufacturing facilities that adversely raises cost. (Errachid et al. 2001; Johnson et al. 1992) Micron-sized wires (*i.e.* Pt, Au, Ag and carbon) are cheaper alternatives,(Ahmad et al. 2007; Chen et al. 2002a; Chen et al. 2002b; Oh et al. 2005; Yoneyama et al. 2009) however their output signals typically fall into the sub-nA levels,(Oh et al. 2005) which is close to electronic circuit noise.

Herein we report on the fabrication and characterization of a highly miniaturized biosensor geometry that exhibits extreme sensitivity, while retaining flexibility and ease of fabrication. This is based on three microwires embedded within a flexible insulator, with the sensing

element realized on the severed end, hereby defined as “edge-plane”. The close distances between the working, reference and counter electrodes affords minimal iR drop, while the ultra-thin (25 μm in diameter) working electrode affords 3-D diffusion for effective mass transfer. Electrochemical rebuilding of the Au working electrode together with Pt nanoparticles deposition increased surface area and electro-catalytic activity against H_2O_2 detection. (Qiang et al. 2010) Electrodeposition of *o*-phenylenediamine together with glucose-oxidase (GO_x) afforded glucose detection with improved sensitivity and selectivity (>95%) against common interference species (*i.e.* ascorbic acid, uric acid and acetaminophen). With H_2O_2 and glucose sensitivity of 33 ± 1 and 1.2 ± 0.1 $mA \cdot mM^{-1} \cdot cm^{-2}$, respectively, this sensor configuration constitutes the highest reported sensitivity thus far. The relative small sensor size, high sensitivity, low operational potential and ease of fabrication, renders the edge-plane microsensor geometry as a promising platform for continuous *in vivo* biosensing.

2. Experimental Section

2.1. Materials and Characterization Instrumentation

All chemicals were procured from Aldrich. Polyurethane was purchased from Fluka (product number 81367, Slectophore). Gold (25 μm in diameter), silver and platinum/iridium (each 125 μm in diameter and coated with Teflon) wires were obtained from World Precision Instruments Inc., in Sarasota, FL. Poly(dimethylsiloxane) (PDMS) Kit (SYLGARD 184) and PE tubing (Intramedic PE50) were purchased from Fisher Scientific. Scanning electron microscopic (SEM) images were collected on a JEOL JSM-6335F SEM equipped with a cold cathode field emission source, operating at 10 kV and working distance of 14.4 mm. All electrochemical experiments were carried out using a CHI 1030 electrochemical workstation.

2.2. Fabrication of Edge-Plane Microsensors

The configuration of the edge-plane microsensor is shown in Figure 1a. Typically, 5-cm long wires were inserted into a PE tube (O.D. = 0.97 mm, I. D. = 0.58 mm), filled with SYLGARD 184 silicone and cured at 120 °C for 1 hour. Subsequently, one end of this tube is cut to expose the tips of the three wires, while on the other end, the Pt/Ir and Ag wires were stripped and connected to larger copper leads.

Fabrication of edge-plane, H_2O_2 sensors—The severed tip was first exposed to 0.1 M HCl, while 0.6 V was applied to the Ag reference electrode for 400 sec to induce AgCl electrooxidation. Consequently, the tip of the sensor was immersed in a 2 M NaOH solution and a square wave potential waveform (from −1.0 V to +0.8 V) was applied for 800 sec to the Au working electrode. (Huang et al. 2009a) Following this, the tip was rinsed and immersed in a 10 mM H_2PtCl_6 / 0.1 M HCl solution and a bias of −0.05 V was applied to the working electrode for 60 sec. (Qiang et al. 2010)

Fabrication of edge-plane, glucose biosensors—The tip of the edge-plane H_2O_2 sensors, described above) was immersed in a quiescent aqueous acetate buffer (pH 6) containing a 5 mM *o*-phenylenediamine (*o*PD) and 10 mg/ml of glucose oxidase (GO_x) and

was let to equilibrate for 5 min. Subsequently, the working electrode was biased at 0.65 V *vs.* the pre-fabricated Ag/AgCl reference electrode for 35 min to induce *o*PD electropolymerization, (Malitesta et al. 1990) followed by a phosphate saline buffer (PBS) rinse, prior to use. These glucose biosensors were optionally dip-coated with polyurethane (PU) from a 3% (w/w) PU in 98% tetrahydrofuran (THF)/2% dimethylformamide (DMF) (w/w) solution. (Chen et al. 2002b)

2.3. Amperometric experiments

Dynamic range amperometric experiments were performed in a stirred PBS solution (pH = 7.4) under various applied potentials with respect to internally built Ag/AgCl reference electrode at room temperature. For H_2O_2 sensing, after an initial background stabilization period of 200 seconds at the desired biasing potential, the concentration of H_2O_2 was sequentially raised from 100 nM to 2 mM every 50 seconds and the amperometric response was continuously recorded. Similarly, for glucose sensing, after an initial background stabilization period of 400 seconds, the concentration of glucose was sequentially raised from 10 μM to 50 mM every 100 seconds and the amperometric response was continuously recorded.

2.4. Data Analysis

Sensor sensitivities *vs.* bias potential for H_2O_2 and glucose were calculated using linear regression analysis between four concentrations points of analyte (100, 200, 300, and 400 μM for H_2O_2 and 1, 2, 3, and 4 mM of glucose, respectively). The apparent Michaelis-Menten constant (K_m^{app}) of GO_x-based glucose sensors was obtained using the Hill equation (n = 1),(Hale et al. 1991) with the help of Origin 8.0 plotting software. All experiments were repeated in triplicate and the data are presented as mean ± S.D.

3. Results and Discussion

3.1 Edge-plane microsensor geometry

The configuration of the edge-plane microsensor geometry is shown in Figure 1a. Using microelectrodes in microfluidics configurations, our previous research indicated that distances varying from microns to millimeters range between the working, counter and reference electrodes show minimal (less than 5%) effect in sensor performance. (Qiang et al. 2010) Accordingly, for the as cut, edge-plane sensors, inter-electrode distance variability resulted in a similar standard deviation range for H_2O_2 sensitivity (*i.e.* less than 5%). Surprisingly, even though such edge-plane sensor contains a working electrode with diameter of *ca.* 25 μm, it is capable to detect H_2O_2 with 0.23 nA/mM sensitivity at 0.6 V *vs.* the internal Ag/AgCl reference electrode, as shown by the left bar in Figure 2a. This is believed to originate from the 3D diffusion layer, as opposed to a conventional 2D for macrosized electrodes. This together with low background charging and reduced *iR* drop (due to proximal distance of all three electrodes) explains the observed sensitivity enhancement. (Huang et al. 2009b) In order to verify microelectrode behavior, cyclic voltammetric (CV) scanning was performed in $K_3(FeCN_6)$. The sigmoidal shape of the CV curve in Figure 2b(i) illustrates a typical microelectrode response that persists at scan rates as high as 100 mV/sec.

3.2 Performance Enhancement of Edge-Plane Microsensors

The good flexibility, ease of fabrication and excellent mechanical stability of these micron-sized wire electrodes convinced us to further investigate means of increasing edge-plane sensor sensitivity in order to counter the anticipated higher noise levels observed for *in vivo* applications. With the edge-plane cross-section fixed, further enhancement in sensitivity can be achieved by increase in surface area and catalytic activity, as discussed in the Introduction Section. For this we resorted to electrochemical gold-surface rebuilding, which is capable to convert a smooth surface to nanoporous morphology. (Huang et al. 2009a) This is based on repeated etch and re-deposition of Au via exposing the Au working electrode in a 2 M of NaOH solution and applying a square waveform (at +0.8 and −1.0 V at a frequency of 50 Hz for 40,000 pulses, with a total exposure of 800 sec). (Huang et al. 2009a) During the application of positive +0.8 V bias, the Au surface gets oxidized and the gold ions form a soluble complex with OH^-, to be re-deposited in the negative −1.0 V bias interval. During both positive and negative intervals, the generation of oxygen and hydrogen micro-bubbles template the Au re-deposition towards nano-/micro-porous morphology. (Huang et al. 2009a) As this electrochemical rebuilding proceeds, the nanoporous structure advances deeper into the Au electrode. Figure 1b illustrates a representative surface morphology as obtained by scanning electron microscopy (SEM), with pore size in the range of 100 to 500 nm, as previously reported. (Huang et al. 2009a) In order to improve stability and increase electrocatalytic activity, the surface of nanoporous Au working electrode was decorated with Pt nanoparticles by electroplating in 10 mM H_2PtCl_6 at −0.05V for 60 sec. (Qiang et al. 2010) Figure 1c shows the surface morphology of the Pt-coated nanoporous Au working electrode. By comparing the SEM micrographs of Figure 1b and 1c, Pt nanoparticles cover effectively the nanoporous Au surface, albeit decreasing slightly its pore size.

In order to confirm the effect of Pt nanoparticles on the microelectrode behavior of the working electrode, the CV curves of the microsensors based on as cut (i) edge plane, nanoporous Au (NPG) (ii) and NPG with Pt nanoparticles are shown in Figure 2b, when tested in 10 mM $K_3Fe(CN)_6$ and 1 M KCl at a scan rate of 10 mV/s. The introduction of Au nanoporosity, increased significantly the curve separation during forward and backwards scans due to appreciable increase in its surface area, while at the same time retaining the typical steady-state diffusion current of the as cut Au microelectrode (i). (Huang et al. 2009b) However, the redox currents above 0.3 V and below 0.05 V show deviations from the sigmoidal shape, indicative of inherent instability of NPG. Upon nano-Pt decoration, the sigmoidal steady state behavior is recovered over the entire scanned range, which is attributable to the extreme electrochemical stability of Pt and crucial for subsequent sensor applications. In accordance with the SEM results of Figure 1b & 1c, the spacing between the forward and backwards scans decreased slightly as a result of decreased porosity following nano-Pt deposition.

Figure 2a illustrates the sensitivities of these three electrodes to H_2O_2 (at 0.6 V *vs.* Ag/AgCl reference). The initial sensitivity of NPG electrode (ii) increased by 374 fold (86.1 $nA \cdot mM^{-1}$) *vs.* that of the as-cut edge plane Au electrode (i) (*i.e.* 0.23 $nA \cdot mM^{-1}$). However, here it is important to mention that the aforementioned NPG value was obtained immediately after its electrochemical re-building step, and its sensitivity steadily decreased

after each test (*i.e.* after three successive dropped down to 12 % of the aforementioned value). Following nano-Pt decorations, NPG electrodes showed an additional 30% increase in sensitivity (115 $nA \cdot mM^{-1}$) (Figure 2a), or *ca.* 500 times from the as-cut edge-plane Au electrode. Moreover, nano-Pt decorated NPG electrodes demonstrated exceptional stability versus that of NPG electrodes, during both operation and storage in PBS buffer (data not shown).

3.3 Hydrogen Peroxide Detection

H_2O_2 is an important byproduct of many analyte-specific enzymes, as well as a known brain neuromodulator. (Vaddiraju et al. 2010) In order to improve performance of enzymatic biosensors (*i.e.* glucose, lactate, etc.), the operating voltage, dynamic range and detection limit of the edge-plane microsensors needs to be established. Figure 3a shows the sensitivity, background, and signal-to-noise (S/N) ratio of nano-Pt-decorated NPG edge-plane microsensors as a function of oxidation potential. Since, these microelectrodes are operated in the presence of oxygen, a high background current was observed at potentials lower than 0.2 V *vs.* Ag/AgCl, typically associated with oxygen reduction. The sensitivity of nano-Pt decorated NPG microelectrodes increased from 36±2 $nA \cdot mM^{-1}$ at 0.1 V to 162±7 $nA \cdot mM^{-1}$ at 0.3 V, before leveling off at *ca.* 148±10 $nA \cdot mM^{-1}$ at 0.6 V. The largest S/N ratio for H_2O_2 detection was afforded at 0.3 V, even though it was found that the sensor operated at 0.3 V lost 90% of its sensitivity within a few hours of operation due to surface contamination. (Qiang et al. 2010) However, sensors when operated at 0.6 V retained their sensitivity for more than 2 weeks operation, due to the cleaning ability at higher potential as previously reported. (Qiang et al. 2010; Rocklin et al. 1998) Based on this, Figure 3b illustrates the nano-Pt NPG microsensor response as a function of H_2O_2 concentration when operated at 0.6 V *vs.* Ag/AgCl reference. The sensors exhibited a five order linear dynamic range from 100 nM to 20 mM as measured by concentration-step amperometry. The detection limit of these microelectrodes is about 50 nM (S/N>3). The sensor displayed a sensitivity of 33±1 $mA \cdot mM^{-1} \cdot cm^{-2}$ (based on its 490 μm^2 geometric cross-sectional area) at potential as low as 0.3 V which is an order of magnitude higher than that reported in the literature. (Chakraborty and Retna Raj 2009; Hrapovic et al. 2004)

3.4 Glucose Sensor fabrication and calibration

To demonstrate the capability of such nano-Pt decorated NPB microelectrode geometry to glucose sensing, glucose oxidase (GO_x) was electrodeposited onto the working electrode from an aqueous buffer solution containing 10 $mg \cdot mL^{-1}$ GO_x and 5 mM *o*PD solution. (De Corcuera et al. 2005) Typically, glucose oxidase based biosensors are prone to various electrochemical interferences, such as ascorbic acid, uric acid and acetaminophen. (Wang 2007) In general, two venues have been established to reduce electrochemical interferences: (a) reduction of operation potential (i.e. 0.2 – 0.4 V) (Vaddiraju et al. 2010); and (b) use of semipermeable membranes (*i.e.* poly(*o*-phenylenediamine) (P*o*PD)(De Corcuera et al. 2005), polypyrrole (Singh et al. 2009), polyphenol (Chen et al. 2002b), etc.) to selectively block diffusion of large molecules towards the working electrode surface. Despite decrease in sensitivity, the overcoating of nano-Pt decorated NPG microelectrodes with electropolymerized films prevents catalytic site poisoning as in the case of H_2O_2 detection at 0.3 V.

By entrapping GO_x enzyme within P*o*PD membranes, both venues for interference reduction can be combined. With this in mind, we investigated the selectivity (*S*) of the nano-Pt decorated NPG microelectrode as a function of applied potential based on the Equation (1), where i_{glu} and i_{AP} are the amperometric currents observed at 5.6 and 0.1 mM of glucose and acetaminophen (AP), respectively.

$$S=\frac{i_{glu}}{i_{glu}+i_{AP}} \quad \text{Equation (1)}$$

Figure 4a shows the edge-plane 6.1±0.5 nA·mM^{-1} (or 1.2±0.1 mA·mM^{-1}·cm^{-2} based on surface normalization) is observed at 0.5 V, which microsensor sensitivities against glucose and acetaminophen (AP) (left ordinate) as well as selectivity (*vs.* AP, from eq. 1) (right ordinate), as a function of applied potential. The glucose sensitivity increases with increasing potential from 0.2 V to 0.3 V and remained almost constant from 0.3 to 0.6 V *vs.* Ag/AgCl. The highest glucose sensitivity of is 6 fold larger than previously reported values. (De Corcuera et al. 2005), (Chen et al. 2002b) Such high sensitivity is attributed to: (i) efficient mass transfer due to microelectrode 3D diffusion layer; (McMahon et al. 2005) (ii) nanoporous Pt-Au structure that provides high surface area; and (iii) intimate contact between conductive surfaces and GO_x through an ultra-thin, electrically conducting P*o*PD polymer matrix. (Trojanowicz et al. 1995) Such high sensitivity at 0.5 V comes at minimal expense in selectivity (*i.e.* 96.0% versus 99.5% at 0.3 V) (Figure 4a). This originates from the fact that the sensitivity of AP decreased by *ca.* 90%, from 12±2 to 1.3±0.5 nA·mM^{-1} from 0.5 to 0.3 V *vs.* Ag/AgCl.

Figure 4b shows the amperometric response of the sensor as a function of glucose concentration at both 0.3 and 0.6 V *vs.* Ag/AgCl. The sensor exhibited a linear dynamic range for glucose detection from 10 μM to 4 mM (see insert of Figure 4b), with a detection limit estimated at 3 μM at 0.6 V, based on S/N ≥ 3. For glucose concentrations above 4 mM, the amperometric response of this sensor started to deviate from linearity, owing to the well-known oxygen dependence of GO_x-based biosensors. (Vaddiraju et al. 2010) Consequently, the Michaelis-Menten equation was used to describe the GO_x kinetics in the particular sensor geometry with K_m^{app} of 25 and 17 mM and maximum current (I_{max}) of 98 and 52 nA for biasing at 0.6 and 0.3 V, respectively.

While the K_m^{app} value of 25 mM at 0.6 V is slightly larger that the maximum physiological glucose lever reported for hyperglycemic patients (*i.e.* 22 mM), the linearity up to 22 mM if far from optimum. In order to further improve on linearity, we applied a diffusion limiting membrane, via dip-coating the sensor in a 3% w/w polyurethane (PU) dissolved in THF/DMF (98% / 2%) solution. (Chen et al. 2002b) Figure 4c shows the amperometric response of PU-coated sensor as a function of glucose concentration. For 0.6 V operational potential, the K_m^{app} increased by 8 times to 134 mM compared to the uncoated sensors. This was accompanied with a near 3-fold decrease in sensitivity, from 3.4 to 1.2 nA·mM^{-1}, owing to limitation of the glucose flux by the PU membrane. (Chen et al. 2002b) Similar results are obtained for 0.3 V operational potential, with K_m^{app} of 75 mM and sensitivity of 1.1 nA·mM^{-1}.

Figure 4d illustrates the amperometric curve of the PU-coated edge-plane microsensor to sequential addition of glucose as well as other typical interfering species such as uric acid (UA), ascorbic acid (AA) and AP when operated at 0.3 V. As desired, the sensor responded quickly to glucose but displayed negligible response to three 0.1 mM additions of AP, AA and UA, respectively, exhibiting selectivity of greater than 95%.

The superior performance of edge-plane microsensors begs the question on how this stacks up against other sensor designs. Table 1 illustrates a comparative tabulation of sensor sensitivity, limit of detection (LOD), linear range and operational potential of various electrochemical glucose sensing geometries based on GO_x enzyme. In terms of operational voltage, most of the reported sensor geometries in Table 1 operate around 0.7 V. Our sensors (both without and with PU outer coating) respond to a bias potential as low as 0.3 V. In terms of sensitivity, to the best of our knowledge, our uncoated sensor is 6 times higher than the best reported value in literature,(De Corcuera et al. 2005) (*i.e.* incorporating P*o*PD/GO_x-coated Pt nanoparticles (PtNPs) onto Pt electrodes, line 2 of Table 1). Such superior performance is also retained using PU diffusion-limiting membrane, which also ranks our sensor *ca.* 20% higher in both sensitivity and linearity than the best reported value. The only drawback of edge-plane sensors is the LOD, which appears to be 1–2 orders of magnitude higher that the best sensor performers in Table 1. This is due to the extreme miniaturization of the working electrode that at low LOD the signal approaches rapidly that of the electronic circuit noise.

4. Conclusions

A novel configuration of electrochemical, biosensors is reported that affords the much needed sensor miniaturization whilst maintaining high sensor performance in terms of sensitivity, selectivity and dynamic range. This is based on three microwires embedded within a flexible insulator, with the sensing element realized on the severed end, hereby defined as “edge-plane”. Owing to the close distance between the working, reference and counter electrodes, this edge-plane microsensors afforded minimal iR drop, 3-D diffusion for effective analyte mass transfer as well as microelectrode behavior. These features together with the electrochemical rebuilding of the Au working electrode and consequent Pt nanoparticles deposition resulted in a 500 fold increase in sensor sensitivity towards H_2O_2. Similarly, electrodeposition of *o*-phenylenediamine in the presence of glucose-oxidase (GO_x) afforded glucose detection with more than 95% selectivity against common interference species (*i.e.* ascorbic acid, uric acid and acetaminophen), while maintaining sensitivities as high as 1.2 $mA{\cdot}mM^{-1}{\cdot}cm^{-2}$ which constitutes the highest reported sensitivity thus far. In addition, these edge-plane glucose microsensors displayed a linear response range well above 30 mM glucose with a limit of detection as low as 3 μM. Such enhanced behavior together with the ease to attain and scale-up the production of micron-sized electrodes with nanostructured porosity renders the edge plane geometry as a promising platform for next generation biosensors.

Acknowledgments

Financial support for this study was obtained from AFOSR FA9550-09-1-0201, NIH ES013557, NIH/NHLBI 1-R21-HL090458-01, Telemedicine and Advanced Technology Research Center (TATRC) at the U.S. Army Medical

Research and Material Command (USAMRMC) (Award No. W81XWH-09-1-0711) and National Institute of Biomedical Imaging & Bioengineering award (R43EB011886).

References

Ahmad F, Christenson A, Bainbridge M, Yusof APM, Ab Ghani S. Biosens. Bioelectron. 2007; 22:1625–1632. [PubMed: 16934449]

Allen MS. J. Dairy Sci. 2000; 83:1598–1624. [PubMed: 10908065]

Chakraborty S, Retna Raj C. Biosens. Bioelectron. 2009; 24:3264–3268. [PubMed: 19442506]

Chen X, Hu Y, Wilson GS. Biosens. Bioelectron. 2002a; 17:1005–1013. [PubMed: 12392950]

Chen X, Matsumoto N, Hu Y, Wilson GS. Anal. Chem. 2002b; 74:368–372. [PubMed: 11811410]

De Corcuera JIR, Cavalieri RP, Powers JR. J. Electroanal. Chem. 2005; 575:229–241.

Erlebacher J, Aziz MJ, Karma A, Dimitrov N, Sieradzki K. Nature. 2001; 410:450–453. [PubMed: 11260708]

Errachid A, Ivorra A, Aguilo J, Villa R, Zine N, Bausells J. Sens. Actuators, B. 2001; 78:279–284.

Fu Y, Li P, Xie Q, Xu X, Lei L, Chen C, Zou C, Deng W, Yao S. Adv. Funct. Mater. 2009; 19:1784–1791.

Hale PD, Boguslavsky LI, Inagaki T, Karan HI, Lee HS, Skotheim TA, Okamoto Y. Anal. Chem. 1991; 63:677–682.

Hrapovic S, Liu Y, Male KB, Luong JHT. Anal. Chem. 2004; 76:1083–1088. [PubMed: 14961742]

Huang W, Wang M, Zheng J, Li Z. J. Phys. Chem. C. 2009a; 113:1800–1805.

Huang XJ, O'Mahony AM, Compton RG. Small. 2009b; 5:776–788. [PubMed: 19340821]

Hye Jin L, Beriet C, Ferrigno R, Girault HH. J. Electroanal. Chem. 2001; 502:138–145.

Johnson KW, Mastrototaro JJ, Howey DC, Brunelle RL, Burden-Brady PL, Bryan NA, Andrew CC, Rowe HM, Allen DJ, Noffke BW, McMahan WC, Morff RJ, Lipson D, Nevin RS. Biosens. Bioelectron. 1992; 7:709–714. [PubMed: 1292518]

Klonoff DC. Diabetes Care. 2005; 28:1231–1239. [PubMed: 15855600]

Kumar CV, Chaudhari A. Microporous Mesoporous Mater. 2003; 57:181–190.

Li CM, Dong H, Cao X, Luong JHT, Zhang X. Curr. Med. Chem. 2007; 14:937–951. [PubMed: 17430145]

Lu J, Do I, Drzal LT, Worden RM, Lee I. ACS Nano. 2008; 2:1825–1832. [PubMed: 19206421]

Malitesta C, Palmisano F, Torsi L, Zambonin PG. Anal. Chem. 1990; 62:2735–2740. [PubMed: 2096737]

McMahon CP, Killoran SJ, O'Neill RD. J. Electroanal. Chem. 2005; 580:193–202.

Oh BK, Robbins ME, Nablo BJ, Schoenfisch MH. Biosens. Bioelectron. 2005; 21:749–757. [PubMed: 16242614]

Patolsky F, Weizmann Y, Willner I. Angewandte Chemie - International Edition. 2004; 43:2113–2117.

Qiang L, Vaddiraju S, Rusling JF, Papadimitrakopoulos F. Biosens. Bioelectron. 2010; 26:682–688. [PubMed: 20655730]

Rocklin RD, Clarke AP, Weitzhandler M. Anal. Chem. 1998; 70:1496–1501.

Singh M, Kathuroju PK, Jampana N. Sens. Actuators, B. 2009; 143:430–443.

Tan Y, Deng W, Chen C, Xie Q, Lei L, Li Y, Fang Z, Ma M, Chen J, Yao S. Biosens. Bioelectron. 2010; 25:2644–2650. [PubMed: 20547053]

Trojanowicz M, Geschke O, Krawczynski vel Krawczyk T, Cammann K. Sens. Actuators, B. 1995; 28:191–199.

Tsai MC, Tsai YC. Sens. Actuators, B. 2009; 141:592–598.

Vaddiraju S, Tomazos I, Burgess DJ, Jain FC, Papadimitrakopoulos F. Biosens. Bioelectron. 2010; 25:1553–1565. [PubMed: 20042326]

Wang J. Chem. Rev. 2007; 108:814–825. [PubMed: 18154363]

Wang YT, Yu L, Zhu ZQ, Zhang J, Zhu JZ, Fan CH. Sens. Actuators, B. 2009; 136:332–337.

Wilson GS, Gifford R. Biosens. Bioelectron. 2005; 20:2388–2403. [PubMed: 15854814]

Wu BY, Hou SH, Yin F, Li J, Zhao ZX, Huang JD, Chen Q. Biosens. Bioelectron. 2007; 22:838–844. [PubMed: 16675215]

Yoneyama Y, Yonemori Y, Murata M, Ohnuki H, Hibi K, Hayashi T, Ren H, Endo H. Talanta. 2009; 80:909–915. [PubMed: 19836572]

You T, Niwa O, Tomita M, Hirono S. Anal. Chem. 2003; 75:2080–2085. [PubMed: 12720344]

Yu X, Munge B, Patel V, Jensen G, Bhirde A, Gong JD, Kim SN, Gillespie J, Gutkind JS, Papadimitrakopoulos F, Rusling JF. J. Am. Chem. Soc. 2006; 128:11199–11205. [PubMed: 16925438]

Zou C, Fu Y, Xie Q, Yao S. Biosens. Bioelectron. 2010; 25:1277–1282. [PubMed: 19926469]

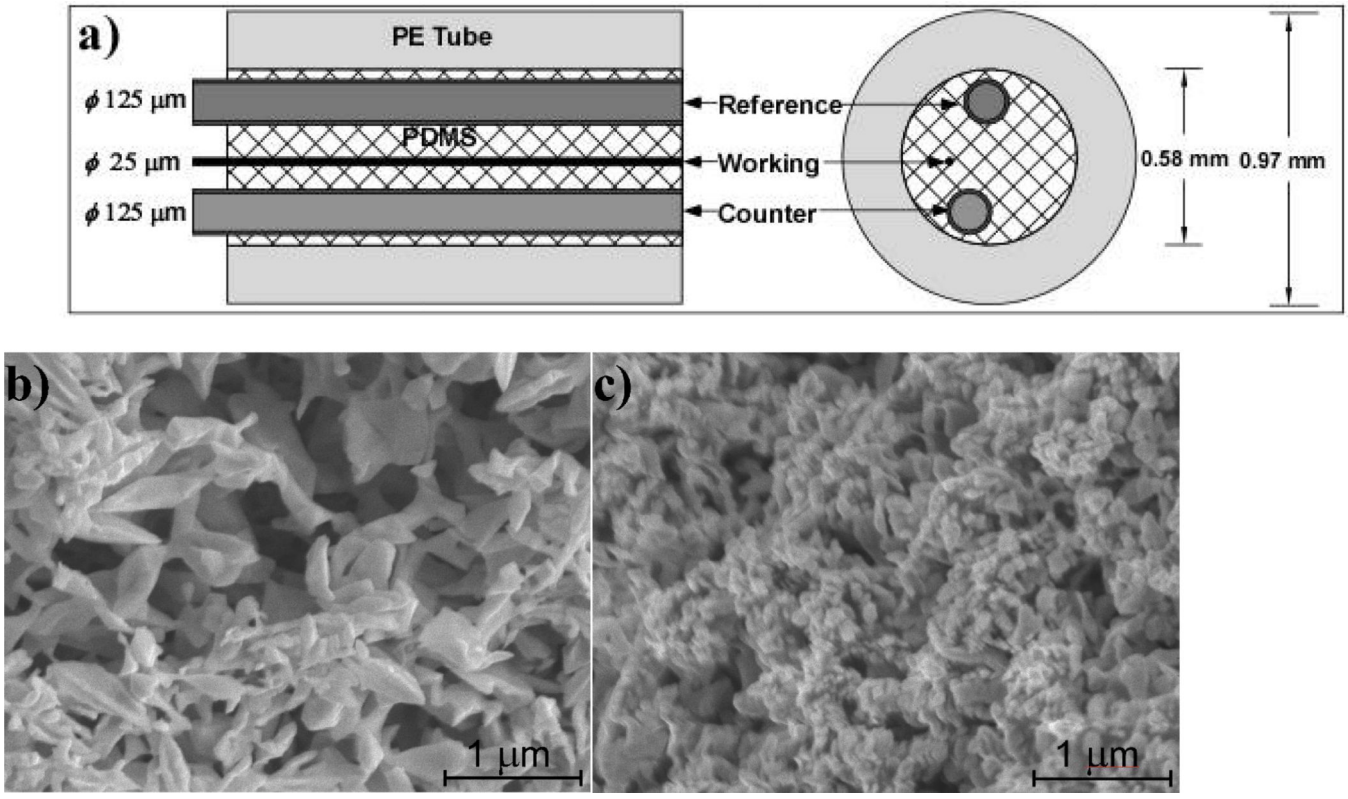

Figure 1.

(a) Configuration of edge-plane microsensor. The diameter (Ø) of all three wires is shown on the left, while the size of the inner and outer diameter of the encasing polyethylene tube is shown on the right. SEM images of the 'electrochemical rebuilt surface' of the Au working electrode, without **(b)** and with **(c)** Pt nanoparticle deposit.

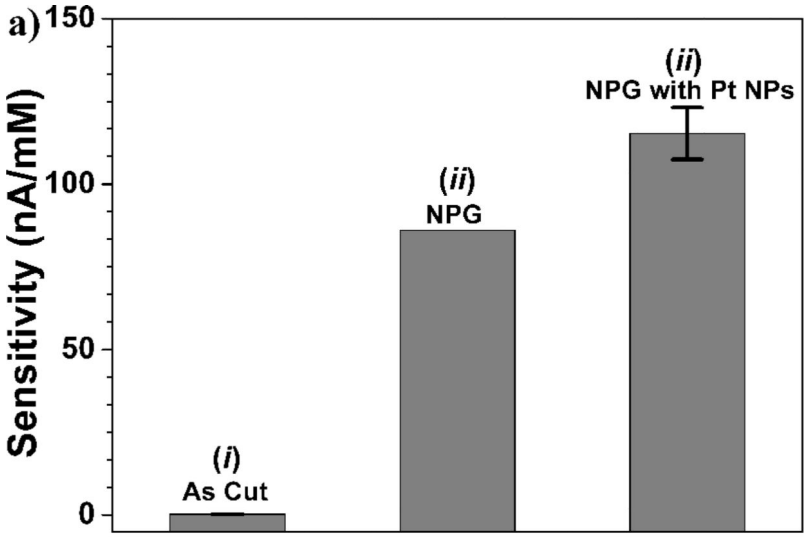

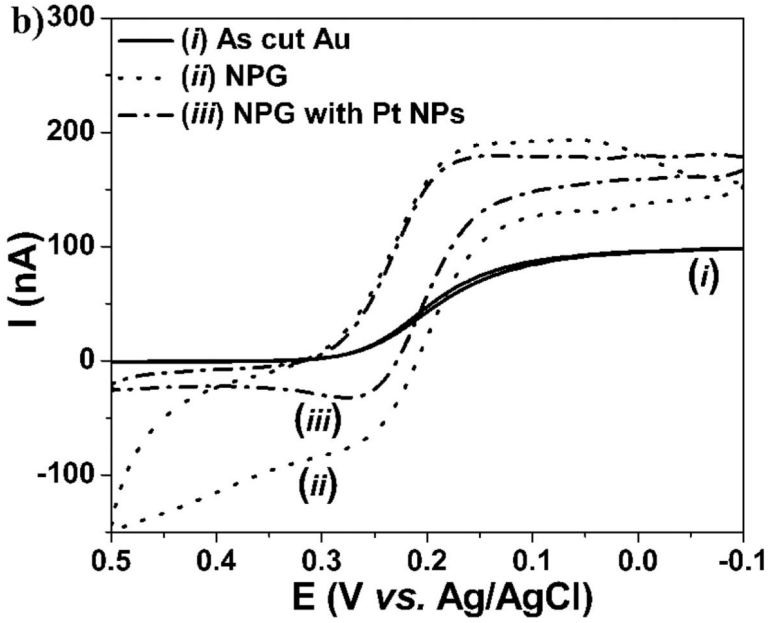

Figure 2.

(a) *In vitro* sensitivity of *(i)* as cut, *(ii)* nanoporous Au (NPG), without and *(iii)* with Pt nanoparticle (NPs) edge-plane sensors for H_2O_2 detection. **(b)** Corresponding cyclic voltammograms in 10 mM $K_3(FeCN_6)$ in 1 M KCl aqueous solution at 10 mV/s scanning rate, with *(i)* and *(iii)* showing microelectrode behavior.

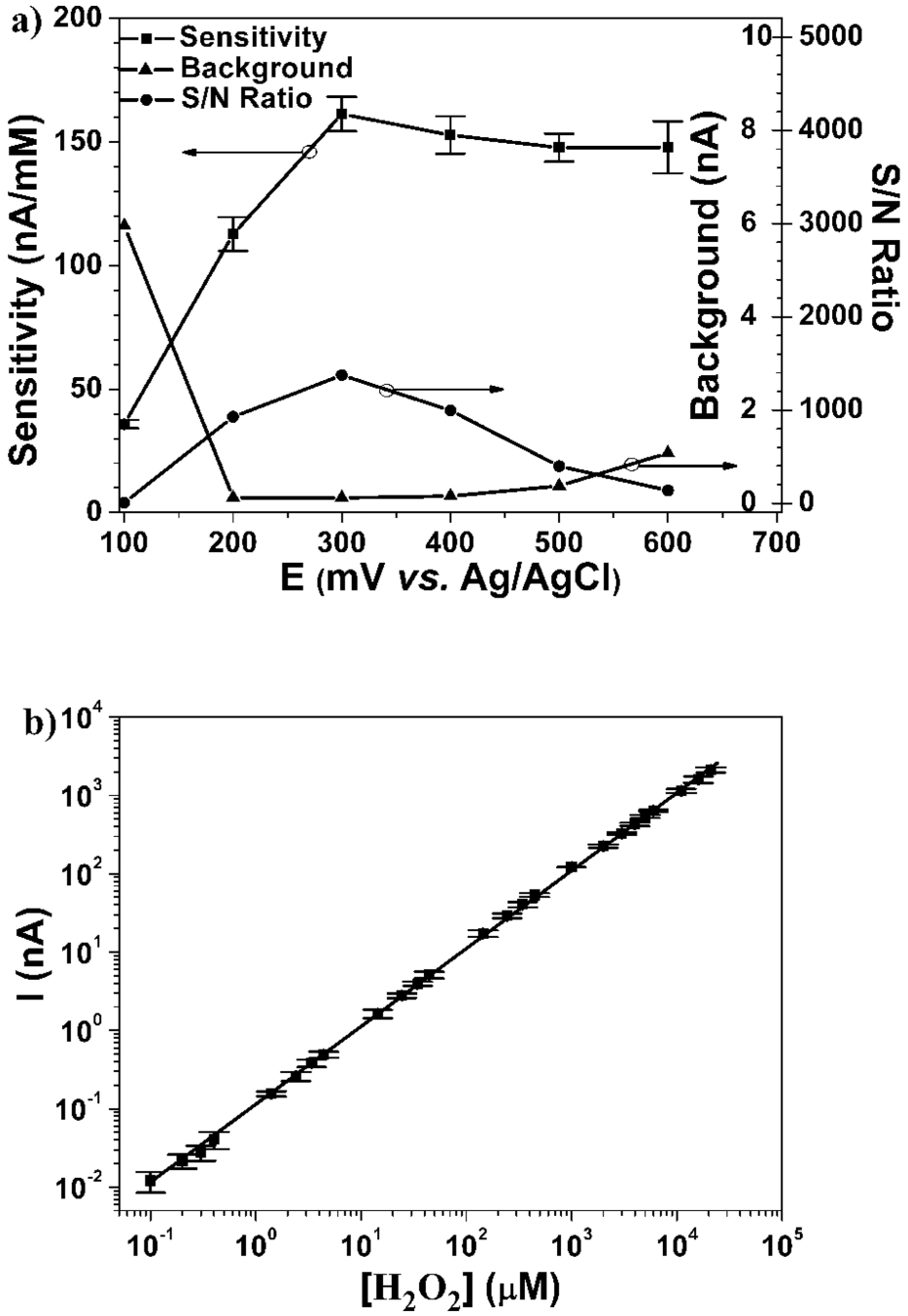

Figure 3.

Edge-plane H_2O_2 sensor performance: **(a)** H_2O_2 sensitivity (left ordinate), background and signal to noise (S/N) (inner and outer sides of the right ordinate, respectively) versus applied potential (against the built-in Ag/AgCl reference electrode, shown in Figure 1). **(b)** Linear dynamic response for H_2O_2 detection at 0.6 V *vs.* Ag/AgCl.

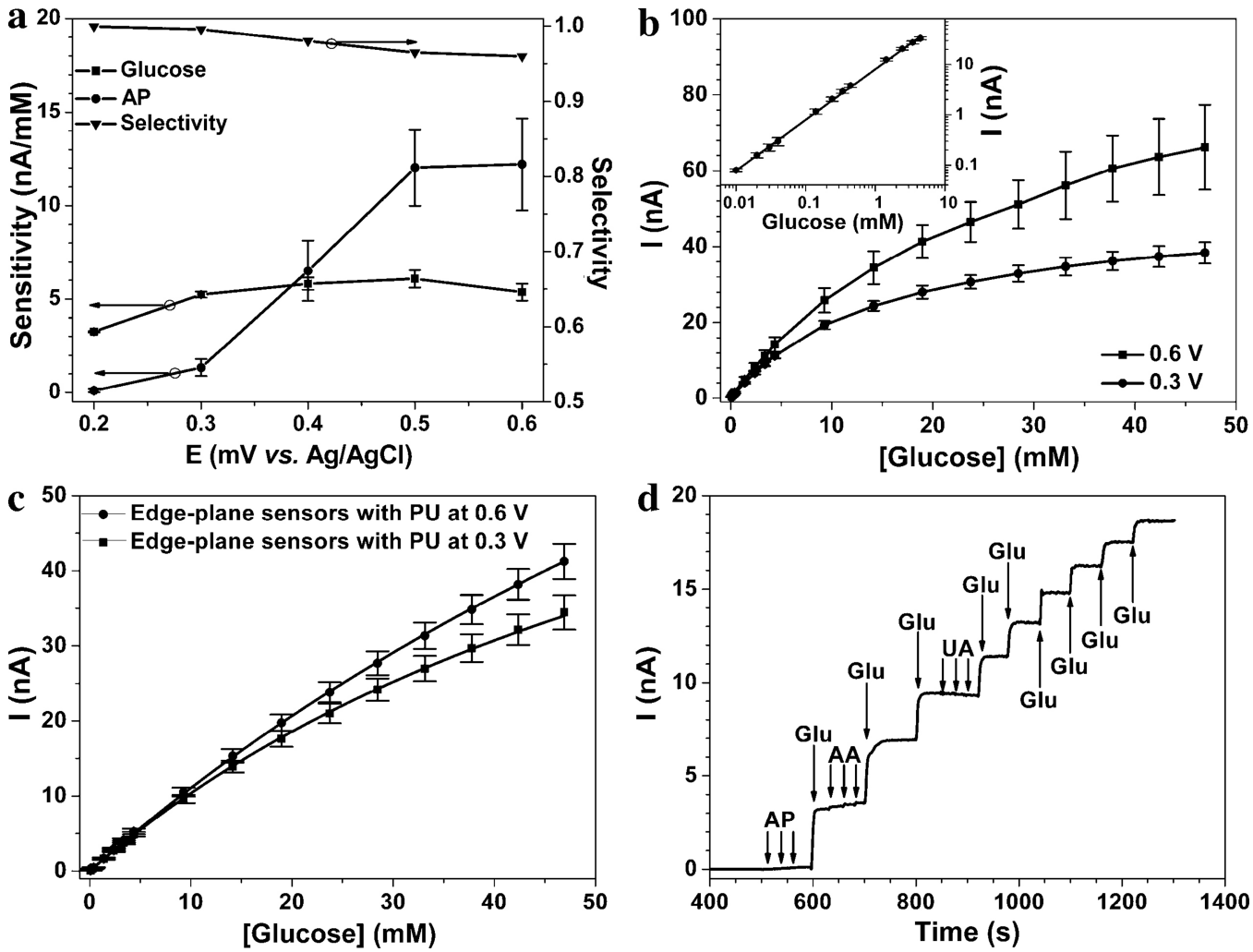

Figure 4.

Glucose detection performance characteristics for edge-plane sensors without **(a & b)** and with **(c & d)** PU membrane: **(a)** Glucose and acetaminophen (AP) sensitivities (left ordinate) and selectivity (glucose against AP calculated as per Eq. 1, right ordinate) at various biasing potential vs. the built-in Ag/AgCl reference electrode. **(b)** Calibration curve glucose detection in PBS (pH = 7.4) at 0.6 and 0.3 V *vs.* Ag/AgCl. Inset shows the enlarged calibration curve at low glucose concentration depicting linear detection range from 10 μM to 4 mM. **(c)** Corresponding calibration curve as (b), in the presence of PU membrane. **(d)** Amperometric response curve for the edge-plane sensor of (c), following the sequential three additions (indicated with arrows) of 0.1 mM of acetaminophen (AP), 5 mM of glucose (Glu), 0.1 mM of ascorbic acid (AA) and 0.1 mM of uric acid (UA).

Table 1

State of the art sensor performance (in terms of sensitivity, linearity, limit of detection (LOD) and operational potential) of various GO_x-based biosensor geometries grown or deposited on a base working electrode, shown in bold.

Working electrode geometry	Sensitivity ($\mu A \cdot mM^{-1} cm^{-2}$)	Linearity (mM)	LOD (μM)	Operational potential (V)	Ref.
Au/PDA-GO_x-PtNPs	129	5.5	0.07	0.7[a]	(Fu et al. 2009)
Pt/PtNPs/P*o*PD-GO_x	198	25	0.3	0.7[b]	(De Corcuera et al. 2005)
GC/PtNPs-xGnP-GO_x	61.5	20	1	0.7[b]	(Lu et al. 2008)
PG/ZnO-MWCNTs/GO_x/PDDA	50	16	0.25	−0.1[b]	(Wang et al. 2009)
Au/PtNPs/CS-GA-GO_x	102	5.3	0.1	0.7[a]	(Tan et al.)
GC/MWCNT-ACS/PtNPs/GO_x	113	10.5	6	0.5[b]	(Tsai and Tsai 2009)
PtDisk/GO_x-GA	20.5	9	3	0.7[b]	(McMahon et al. 2005)
Au/Fe_3O_4-Au-PHDT-GO_x	110	2.6	0.33	0.7[a]	(Zou et al. 2010)
Au/NPG/PtNPs/P*o*PD-GO_x	1200	4	3	0.5[b]	This work
Au/NPG/PtNPs/P*o*PD-GO_x/PU	240	30	50	0.6[b]	This work

(a) versus saturated calomel electrode (SCE);

(b) versus Ag/AgCl.

Abbreviation definitions for various biosensing geometries: "-" and "/" indicate mixtures and sequential deposition, respectively; alumina coated silica (ACS); chitosan (CS); glutaraldehyde (GA); glassy carbon (GC); multi-walled carbon nanotubes (MWCNTs); nanoporous gold (NPG); polydopamine (PDA); poly(diallyldimethylammonium chloride) (PDDA); pyrolytic graphite (PG); poly(1,6-hexanedithiol) (PHDT); poly(*o*-phenylenediamine) (P*o*PD); platinum nanoparticles (PtNPs); polyurethane (PU); exfoliated graphite nanoplatelets (xGnP);.